Journal of Radioanalytical and Nuclear Chemistry (2022) 331:5129–5135
https://doi.org/10.1007/s10967-022-08559-9

Neutron tomography of a highly irradiated spallation target rod

Pavel Trtik[1] · Jörg Welte[1] · Okan Yetik[1] · Sven Grünberger[1] · August Kalt[1] · Jan Hovind[1] · Bertrand Blau[1]

Received: 22 April 2022 / Accepted: 8 September 2022 / Published online: 23 September 2022

Abstract
We performed tomographic investigation of the most heavily perturbed (thus highly radioactive) rod and its pristine/unirradiated replicate from the target No. 12 of the Swiss neutron spallation source (SINQ). The tomographic dataset reveals the 3D re-distribution of the lead filling inside the irradiated Zircaloy tube. The change in the linear attenuation coefficient of both the lead filling and the Zircaloy tube of the irradiated rod (due to the presence of the entrapped spallation products) in comparison with the pristine/unirradiated material is quantified. The dataset provides valuable input for the enhancement of safety and efficiency of future spallation targets at SINQ.

Keywords Neutron tomography · Radioactive · Irradiated · Spallation · Target · Dysprosium · Imaging plate · NEURAP · NEUTRA · SINQ

Introduction

The Swiss neutron spallation source (SINQ) [1] at the Paul Scherrer Institut (PSI) produces free neutrons by means of a target bombarded by an intense 590 MeV proton beam. The SINQ target comprises more than 300 hermetically-sealed Zircaloy tubes filled with lead up to 90 percent of its inner volume (see Fig. 1). The desired original distribution of lead filling inside the Zircaloy tube is achieved by lead melting and solidification [2]. The distribution of the pristine lead filling in the fully welded tube is then checked by neutron radiography using standard scintillator-camera detector.

The SINQ source is a continuous spallation source and it experiences a large number of short operational interruptions (in the order of fifty thousand over the standard two years of its operational lifetime). These include intentional pauses for the production of ultracold neutrons (so-called UCN-kicks) [3] and unintentional beam interruptions in the production of protons. Even though only a fraction of the incoming proton beam energy is deposited at SINQ [4], the operational pauses lead to cycles of melting and solidification of the lead filling (lead melting point is 600.6 K) in the most heavily thermally loaded rods [5]. The volumetric fraction of the lead inside the rods is only up to 90% which allows for the thermal expansion/contraction of lead during melting and solidification cycles (lead density in molten state 10.66 g/cm^3, lead density at 25 K 11.34 g/cm^3). Though, it has been recently demonstrated using neutron radiography of inactive target rods subjected to heating/cooling cycles [6] that such repeated melting/solidification process leads to redistribution of the lead filling inside the Zircaloy tubes.

In this process, the centre part of the target rod gets progressively filled up fully with the melted/solidified lead filling, while the solid lead parts of the filling at the ends of the tube shrink progressively towards the centre of the rod. This poses a potential risk to the evolution of cracks in the irradiated Zircaloy tubes due to the build-up of hydrostatic pressures in fully filled up parts of the rods and, therefore, to the safety of the target [7]. The detailed knowledge about the distribution of lead inside the irradiated target rods is therefore of crucial importance for both the safe operation of the source and for the optimization of the source efficiency.

The SINQ targets at the end of its lifetimes represent very highly radioactive samples (dose rate ~ 100 Sv/h). The non-destructive investigation of the inner structure of highly radioactive materials using neutrons is demanding and is routinely performed only at a very few facilities worldwide (e.g. [8–11]). In Paul Scherrer Institute, such samples can be imaged at the NEUTRA thermal neutron imaging beamline [12] by means of NEURAP—a dedicated set-up for highly radioactive materials. Applications of NEURAP for imaging

✉ Pavel Trtik
pavel.trtik@psi.ch

[1] Paul Scherrer Institut, Forschungsstrasse 111, 5232 Villigen, Switzerland

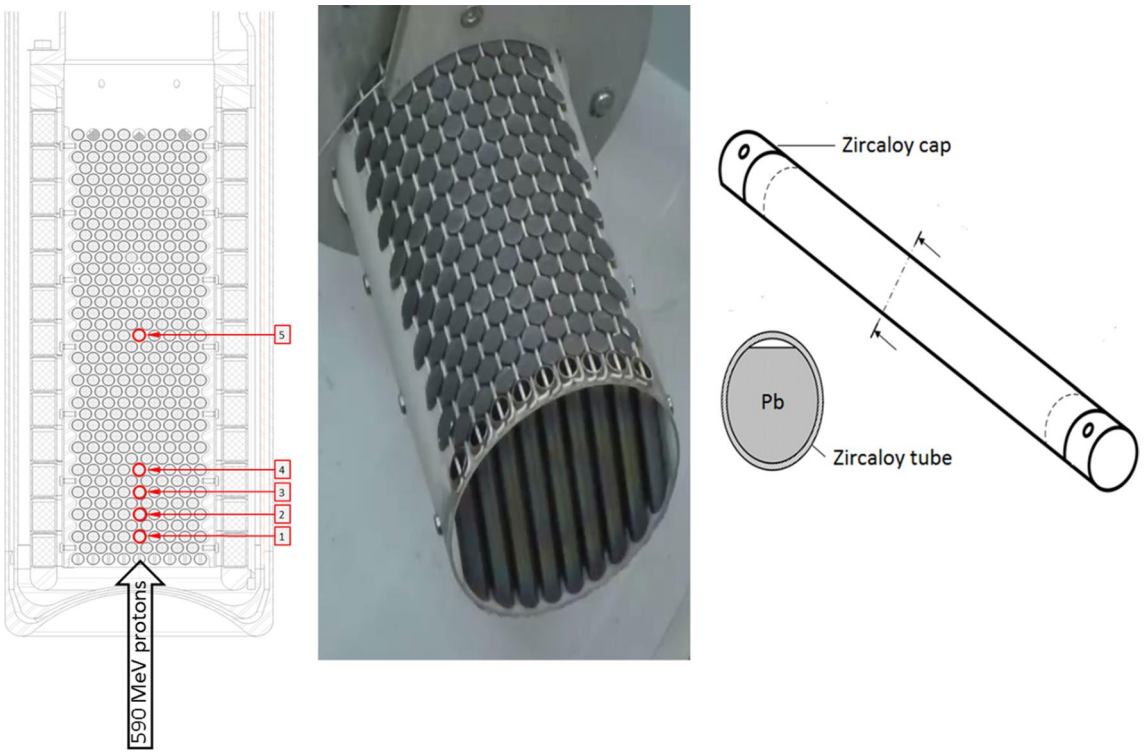

Fig. 1 (Left) Cross-section of the SINQ neutron spallation target No. 12 showing the direction of the incoming protons, (middle) the photograph of the target with stripped casing, (right) a sketch of the single Zircaloy target rod showing the original extent of the lead filling. The original outer diameter of the Zircaloy tube was 10 mm, the rod full length including the Zircaloy caps is 127.5 mm

of radioactive materials have been recently reviewed by Lehmann et al. [13]. It should be noted that all but one [14] of the applications in the above mentioned review are limited to 2D radiography. In this pioneering work we present the first attempt for tomographic investigation using a reasonably high number of projections with the goal of the visualization of the lead distribution in the most perturbed rod from target No. 12 of the Swiss neutron spallation source (SINQ).

Experimental

The SINQ target No. 12 has been operated in the years 2016 and 2017 and received the total proton current integral of 5,239 mAh. During that time the target experienced 23,435 UCN-kicks and 13,504 additional unintentional short proton accelerator operational pauses. In September 2020, five rods were removed from the target in a large dedicated hot cell (ATEC) and placed into the NEURAP sample capsule for neutron radiographic investigation. Positions of the investigated rods in the target No. 12 are clearly marked in Fig. 1 left. The radiographies showed major redistribution of lead in the first four rods (Nos. 1–4) while the rod No. 5 exhibited hardly any apparent redistribution of the lead filling.

Based on the radiographic investigations, the rod No. 2 (originally denominated Z4-5) exhibited the largest apparent redistribution of the lead filling (see the arrow in Fig. 2) making it likely the most perturbed rod of the target No. 12 and was thus selected as the sample of interest for the neutron tomographic investigation. The dose rate of the target rod No. 12 measured shortly before the tomographic investigation was equal to 345 mSv/h.

For the tomographic investigation, the target rod No. 2 has been placed at bottom of the NEURAP aluminum sample capsule. In addition, a pristine (unirradiated) Zircaloy replicate rod was placed on the top of the rod No. 2. For the purpose of the assessment of the spatial resolution, a broken piece of spatial resolution test object (gadolinium Siemens star [15, 16], was fitted on the top of the pristine target rod. The tomographic investigation of the two target rods was performed at NEUTRA beamline at measuring position No. 2 (L/D = 365) in April 2021 (see Fig. 3). A set of 27 dysprosium based imaging plates [17] of 40 × 250 mm in size were utilized for the investigation. In the first step, the images of all 27 imaging plates without any sample present in the beam were acquired for the subsequent image normalization. The following temporal sequence was consistently applied for the data acquisition: (1) 15 min pre-erasure, (2) 20 min neutron exposure, (3) 15 min erasure, (4) 90 min self-exposure

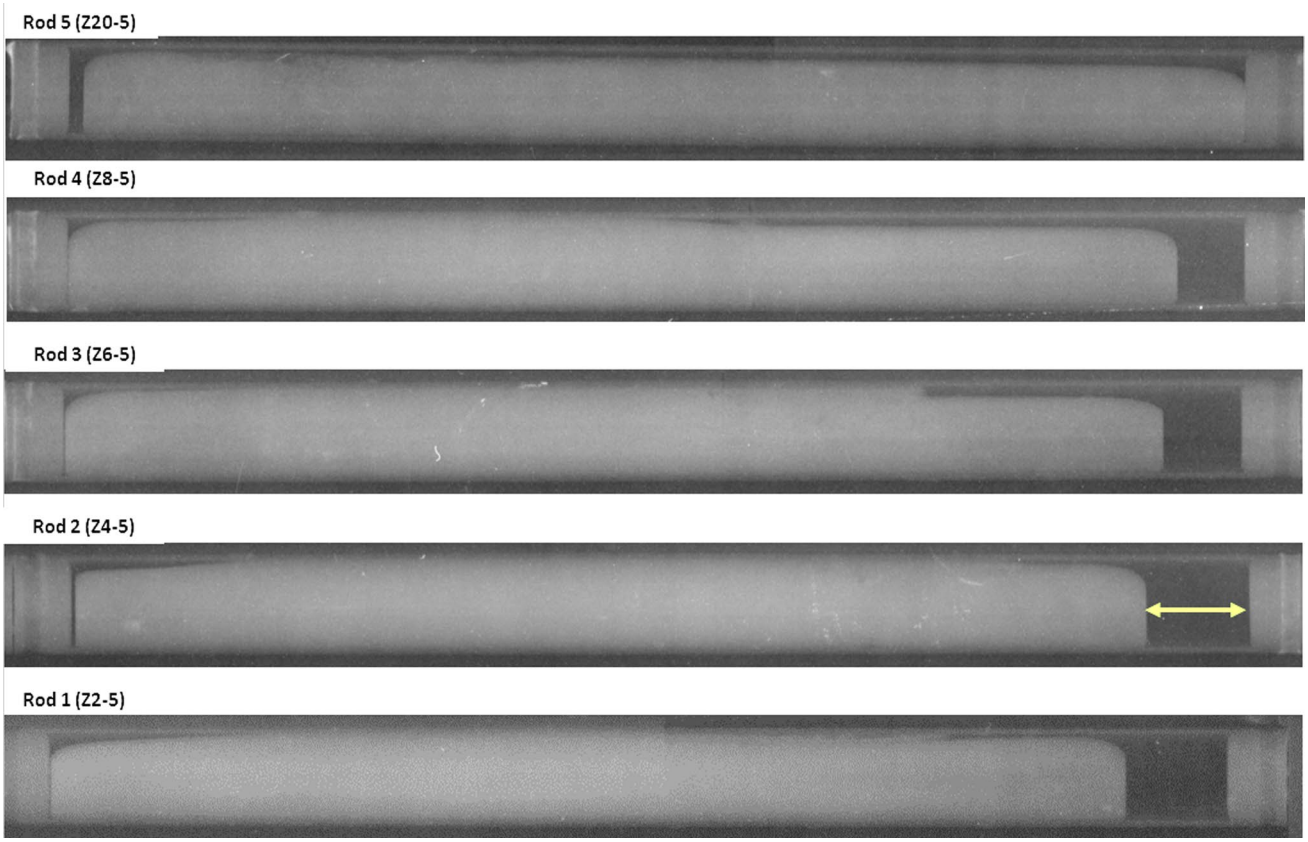

Fig. 2 Neutron radiographies of the highly irradiated five target rods from SINQ target No. 12. The rod diameters equal approximately 10 mm. The rod No. 2 (originally denominated Z4-5) showing the largest redistribution of the lead filling (see the green arrow)

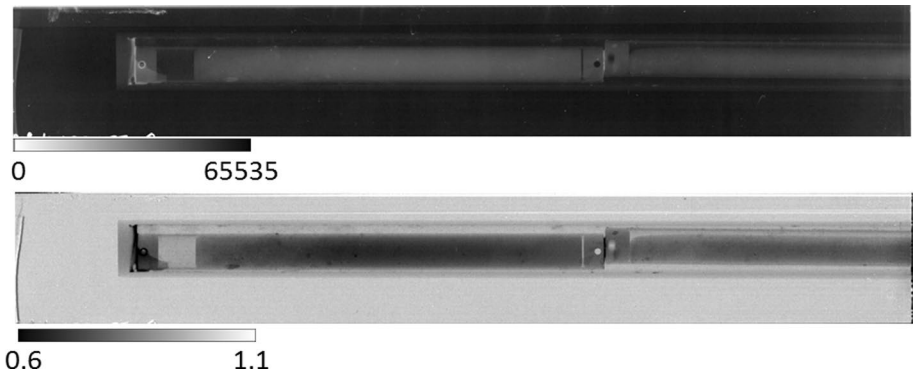

Fig. 3 Original (above) and normalized (below) projection images of the highly radioactive SINQ spallation target rod

followed by immediate scanning of each imaging plate using an imaging plate reader.

The sample capsule has been lowered to the beam position in such a manner that the entire length of the irradiated sample and a lower part of the pristine sample were in the available field of view. The samples were then subsequently scanned in thirty-seven angular positions that were evenly distributed along 180 degrees rotation. The following interleaved acquisition scheme [18] has been applied—0:20:180, 10:20:170, 5:10:175. Taking into consideration the decay time of Dy-165 m (half-life of 2.334 h), it was assured that the same imaging plate was not used more than once within 24 h. The acquisition sequence was completed with an image of the entire pristine sample with gadolinium Siemens star for the check of the spatial resolution.

The total experimental time for the tomographic investigation was approximately 32 h. All the original images were of the size of 9920 × 1440 pixels. The pixel size was equal to 25 µm.

The original projection images were normalized by the corresponding images of the imaging plates without samples. As the imaging plates could not be placed in the imaging plate reader with sufficient (sub-pixel) reproducibility the images were registered to each other based on the area outside the sample using affine registration routine in *Avizo* software [19]. The examples of the original and the normalized image are shown in Fig. 3.

After the normalization all the 37 projection images were manually prealigned and cropped to the size of 7236 × 744 pixels. In the next step, the stack of the normalized images was registered using *StackReg* routine in Fiji software [20]. Due to the fact that the 37 projections are still far from satisfying the sampling theorem, the stack of images was binned by factor 4 × 4 leading to 37 images of 1809 × 186 pixels in size and of the resulting pixel size of 100 µm.

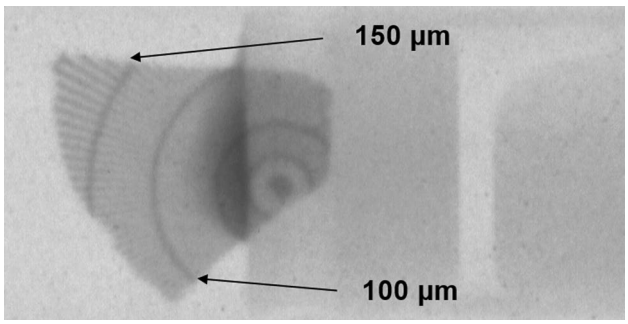

Fig. 4 Image of a part of the gadolinium Siemens star resolution test pattern showing approximately 120 µm spatial resolution (single spoke size)

The dataset has been reconstructed using a standard filtered back projection algorithm using *Muhrec* software [21] (Hamming filter, cut-off = 0.5) thus providing the 3D map of linear attenuation coefficients [22]. Wavelet-FFT ring artifact removal algorithm [23] was applied during the reconstruction. The reconstructed dataset was post-processed using ISS edge preserving filter [24] using *Kiptool* software [25].

Results and discussion

As this is the first tomographic investigation of highly radioactive samples using the NEURAP insertion device that is based on reasonably high number of projections, the spatial resolution of the technique is discussed first here. The visual assessment of the image of a part of the gadolinium Siemens star [15, 16] at the top of the pristine sample revealed approximately 120 µm spatial resolution for a single spoke size (240 µm line pair)—see Fig. 4. At the same time, a Zircaloy edge response function from the 3D dataset was evaluated to be approximately 300 µm (10–90% of the edge response distance).

Figure 5 shows the reconstructed vertical slice of the tomographic dataset from approximately axial position of the both target rods as well as the reconstructed horizontal/axial slices of both the rods. The observed attenuation coefficient of pristine lead ($\Sigma_{pristine\_lead} = 0.21\ cm^{-1}$) does not differ significantly from that of the pristine Zircaloy ($\Sigma_{pristine\_Zircaloy} = 0.20\ cm^{-1}$). The average linear attenuation coefficient of lead filling of the highly radioactive sample changes significantly along the horizontal position of the target (see Fig. 6). The highest attenuation coefficient

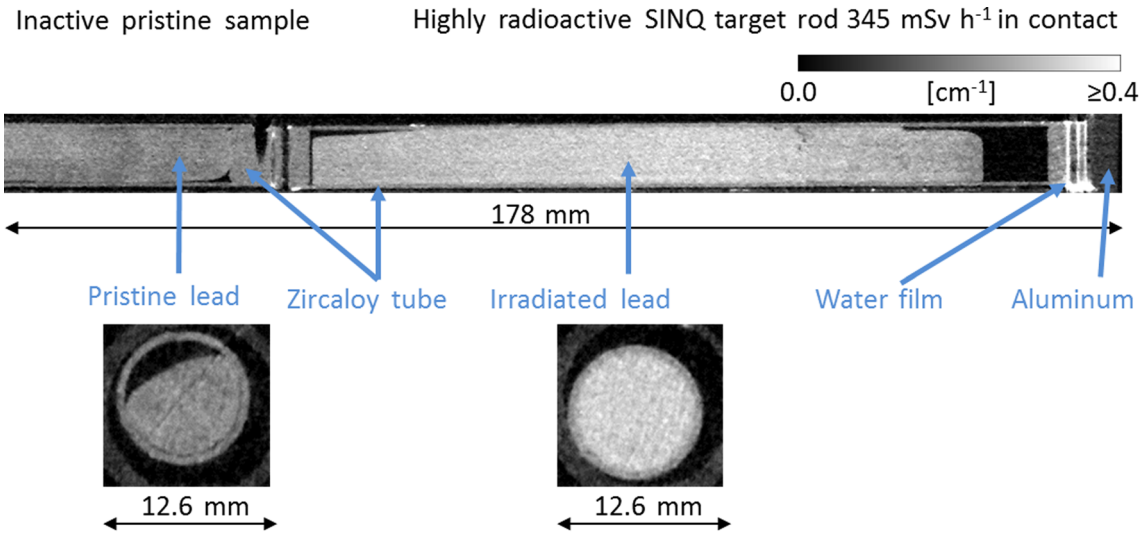

Fig. 5 Vertical slice from the tomographic reconstruction of (top right) highly radioactive SINQ target rod and (top left) a part of the pristine unirradiated target rod. The axial slice of the pristine/unirradiated sample (bottom left) and the axial slice of the highly irradiated sample (bottom right) showing the clear difference in the linear attenuation coefficients betwen the irradiated and the pristine material

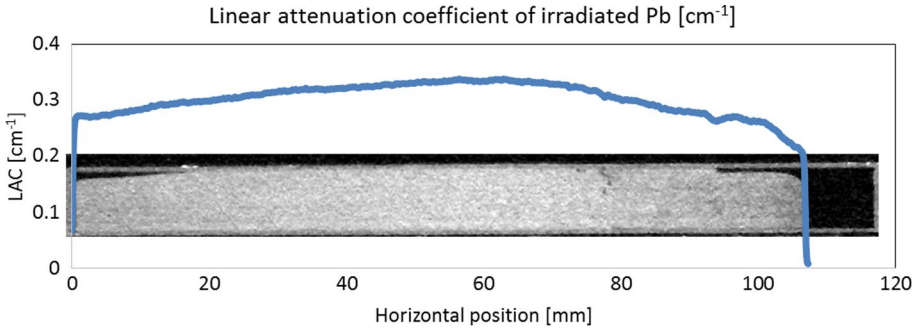

Fig. 6 The linear attenuation coefficient of lead in the highly activated SINQ spallation target rod plotted as the function of the horizontal position of the rod

of the lead filling ($\Sigma_{irradiated\_lead} = 0.33\ cm^{-1}$) is observed approximately at the centre of the rod (see Fig. 5 bottom right) which represents more than 57 percent increase with respect to the pristine material. This is consistent with the fact that the centre of the highly radioactive rod received the highest dose of protons and therefore is expected to exhibit the highest level of spallation products (e.g. hydrogen) exhibiting superior neutron cross-section than that of the lead. Likewise, the increase in linear attenuation coefficient is observed also in the case of the highly radioactive Zircaloy tube ($\Sigma_{irradiated\_Zircaloy} = 0.25\ cm^{-1}$). However, this increase is relatively lower than the corresponding relative increase in the linear attenuation coefficient of lead (25 percent for Zircaloy versus more than 57 percent for lead). This observation is, however, consistent with the lower proton capture cross-section of zirconium than that of the lead. The linear attenuation coefficient of aluminum in the NEURAP's 16 mm-diameter sample capsule equals ($\Sigma_{aluminum} = 0.08\ cm^{-1}$).

Thanks to the relatively low noise level in the reconstructed datasets several material phases can be easily rendered. Figure 7 presents the 3D renderings of the distinguishable material phases in the highly radioactive target rod. The presence of water (blue phase in Fig. 7 top left)—likely due to the insufficient drying of the sample capsule during the preceding decontamination procedure—was unexpected. Several droplets of the decontamination liquid can be observed both on the outer wall of the Zircaloy tube as well as on the inner wall of the 16-mm-diameter aluminum sample capsule.

The shape of the Zircaloy rod has been revealed in 3D and its thickness analysis can be thus performed at an arbitrary cross-section. The approximately 100 µm larger thickness of the rod in the centre in comparison with the thickness at

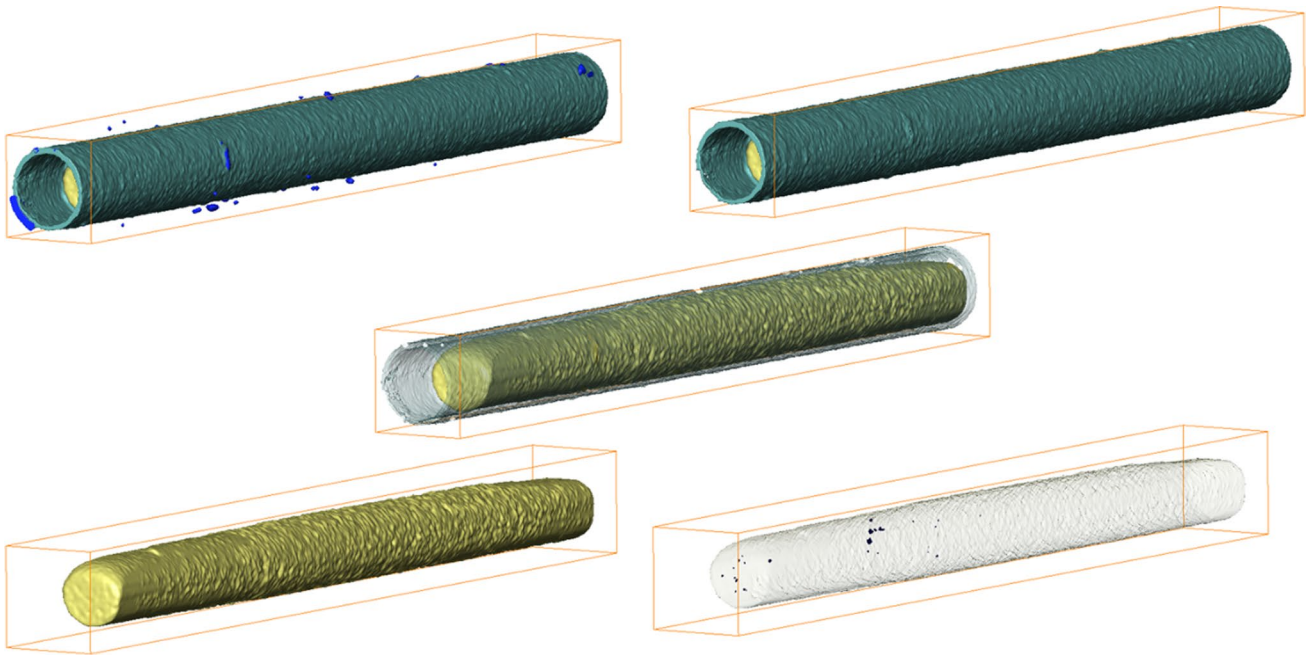

Fig. 7 3D renderings of the identified material phases: blue—water droplets in the sample capsule, dark green—Zircaloy tube, yellow—lead filling, black—porosity in the lead filling. The size of the visualized bounding boxes is equal to 12.6 × 12.3 × 117 mm

the rod's ends had been observed and was confirmed by the tactile measurements performed in the ATEC hot cell.

Regarding the shape of the redistributed lead filling, the tomographic dataset revealed that approximately 50 mm of the central part of the highly irradiated rod has been fully filled with the lead while the lead filling shrunk approximately 10 mm one side of the rod. The defects/pores in the lead filling—otherwise undetectable by radiography only—were revealed in the tomographic datasets as well (see Fig. 7 bottom right).

In general, the presented investigation offers the first NEURAP based tomographic dataset of highly radioactive material which allows a quantitative analysis based on the derived linear attenuation coefficients (LAC). The lower than expected values of the derived linear attenuation coefficients are to be expected due to the fact that no scatter correction [26, 27] could be applied during acquisition. The observed increase in LAC of Zircaloy due to the irradiation corresponds well with the expected level of implanted spallation products (e.g. 6600 appmH in the SINQ target No. 11) [7].

The homogeneous distribution of linear attenuation coefficient along the perimeter (see Fig. 5 bottom right) suggests that no areas of inhomogeneous hydrides accumulation were present in the radioactive target rod. This is consistent with the recent results based on the high-resolution neutron imaging [28, 29] of SINQ target rod material [30]. As much as this diminishes the concerns about the extent of the local embrittlement, the large area of the rod fully filled with the lead together with the observed increase in the rod's thickness in its centre part gives reasons for safety concerns [7].

Conclusions

The first tomographic investigation of highly radioactive (345 mSv/h) SINQ spallation target rod using a reasonably large number of projections was performed. The obtained neutron tomography dataset is pioneering in numerous ways and goes qualitatively beyond any tomography of highly radioactive object made so far using the NEURAP technique. It reveals in 3D the re-distribution of the lead filling inside the rod as well as the precise shape of the deformed target rod (including the approximately 100 µm increase in the thickness of its centre part). Thanks to the applied image normalization trustworthy values of the linear attenuation coefficients of the materials are derived. The change in the linear attenuation coefficient of the lead filling—probably thanks to the presence of the entrapped spallation products—in comparison with the pristine lead was quantified. The dataset will be used in the future as a valuable input for possible design improvements of future SINQ targets both in the direction of its safety and its efficiency.

Acknowledgements This work is based on experiments performed at the Swiss spallation neutron source SINQ, Paul Scherrer Institute, Villigen, Switzerland. The first author would like to express sincere gratitude to Drs Sam Glover and Steve LaMont for organizing the MARC-XII conference in 2022 and to the big island of Hawaii for the positive energy given during the writing the original draft of this manuscript. The first author would like to express sincere thanks to Dr Aaron Colldeweih (PSI) for the useful discussion of the topic. The authors would like to express their sincere thanks to colleagues from ATEC hot cell and SINQ's radiation safety groups at PSI for their invaluable assistance during the experiments. Last but not the least, the authors would like to thank two anonymous reviewers for the revisions that helped perfecting the manuscript.

Funding Open Access funding provided by Lib4RI – Library for the Research Institutes within the ETH Domain: Eawag, Empa, PSI & WSL.

References

1. Blau B et al (2009) The Swiss Spallation Neutron Source SINQ at Paul Scherrer Institut. Neutron News 20(3):5–8. https://doi.org/10.1080/10448630903120387
2. Wagner W, Blau B, Heyck H, Lehmann E, Thomsen K (2010) Status and development of the Swiss spallation neutron source (SINQ). In: ICANS XIX, 2010
3. Anghel A et al (2009) The PSI ultra-cold neutron source. Nucl Instrum Methods Phys Res Sect A Accel Spectrom Detect Assoc Equip 611(2–3):272–275. https://doi.org/10.1016/j.nima.2009.07.077
4. Haj Tahar M, Kiselev D, Knecht A, Laube D, Reggiani D, Snuverink J (2022) Probing the losses for a high power beamitle. https://arxiv.org/pdf/2205.12536.pdf, submitted
5. Sobbia R, Dementjevs S, Joray S, Wohlmuther M (2013) Thermomechanical investigations of the sinq 'cannelloni' target. In: IPAC 2013: proceedings of the 4th international particle accelerator conference, 2013, pp 3445–3447
6. Wohlmuter M, Dementjevs S, Vontobel P, Hovind J, Trtik P, Lehmann EH (2020) Investigation of sinq (Lead/zircaloy) spallation target structures by means of neutron imaging techniques. Mater Res Proc 15:287–291. https://doi.org/10.21741/9781644900574-45
7. Dai Y et al (2021) Post-irradiation examinations of sinq target-11. Mater Sci Forum 1024:41–52. https://doi.org/10.4028/www.scientific.net/MSF.1024.41
8. Jenssen HK, Oberländer BC, Beenhouwer JD, Sijbers J, Verwerft M (2014) Neutron radiography and tomography applied to fuel degradation during ramp tests and loss of coolant accident tests in a research reactor. Prog Nucl Energy 72:55–62. https://doi.org/10.1016/j.pnucene.2013.11.001

9. Craft AE et al (2015) Neutron radiography of irradiated nuclear fuel at Idaho National Laboratory. Phys Procedia 69:483–490. https://doi.org/10.1016/j.phpro.2015.07.068
10. Vogel SC et al (2020) Advanced postirradiation characterization of nuclear fuels using pulsed neutrons. Jom 72(1):187–196. https://doi.org/10.1007/s11837-019-03849-2
11. Singh JL et al. (2011) Non destructive evaluation of irradiated nuclear fuel pins at cirus research reactor by neutron radiography. In: NDE 2011, proceedings of the indian national seminar & exhibition on non-destructive evaluation, pp 8–12
12. Lehmann EH, Vontobel P, Wiezel L (2001) Properties of the radiography facility NEUTRA at SINQ and its potential for use as European reference facility. Nondestruct Test Eval 16(2–6):191–202
13. Lehmann E, Thomsen K, Strobl M, Trtik P, Bertsch J, Dai Y (2021) NEURAP—a dedicated neutron-imaging facility for highly radioactive samples. J Imaging 7(3):57. https://doi.org/10.3390/jimaging7030057
14. Vontobel P et al (2006) Post-irradiation analysis of SINQ target rods by thermal neutron radiography. J Nucl Mater 356(1–3):162–167. https://doi.org/10.1016/j.jnucmat.2006.05.033
15. Grünzweig C, Frei G, Lehmann E, Kühne G, David C (2007) Highly absorbing gadolinium test device to characterize the performance of neutron imaging detector systems. Rev Sci Instrum. https://doi.org/10.1063/1.2736892
16. Trtik P et al (2015) Improving the spatial resolution of neutron imaging at Paul Scherrer Institut: the neutron microscope project. Phys Procedia. https://doi.org/10.1016/j.phpro.2015.07.024
17. Tamaki M, Iida K, Mori N, Lehmann EH, Vontobel P, Estermann M (2005) Dy-IP characterization and its application for experimental neutron radiography tests under realistic conditions. Nucl Instrum Methods Phys Res Sect A Accel Spectrom Detect Assoc Equip 542(13):320–323. https://doi.org/10.1016/j.nima.2005.01.156
18. Kaestner A, Münch B, Trtik P, Butler L (2011) Spatiotemporal computed tomography of dynamic processes. Opt Eng. https://doi.org/10.1117/1.3660298
19. Pluim JPW, Maintz JBAA, Viergever MA (2003) Mutual-information-based registration of medical images: a survey. IEEE Trans Med Imaging 22(8):986–1004. https://doi.org/10.1109/TMI.2003.815867
20. Schindelin J et al (2012) Fiji: an open-source platform for biological-image analysis. Nat Methods 9(7):676–682. https://doi.org/10.1038/nmeth.2019
21. Kaestner AP (2011) MuhRec: a new tomography reconstructor. Nucl Instrum Methods Phys Res Sect A Accel Spectrom Detect Assoc Equip. https://doi.org/10.1016/j.nima.2011.01.129
22. Buzug T (2008) Computed tomography. Springer, Berlin
23. Münch B, Trtik P, Marone F, Stampanoni M (2009) Stripe and ring artifact removal with combined wavelet: Fourier filtering. Opt Express. https://doi.org/10.1364/OE.17.008567
24. Kaestner A, Lehmann E, Stampanoni M (2008) Imaging and image processing in porous media research. Adv Water Resour 31(9):1174–1187. https://doi.org/10.1016/j.advwatres.2008.01.022
25. Carminati C, Strobl M, Kaestner A (2019) KipTool, a general purpose processing tool for neutron imaging data. SoftwareX. https://doi.org/10.1016/j.softx.2019.100279
26. Boillat P et al (2018) Chasing quantitative biases in neutron imaging wit scintillator-camera detectors: a practical method with black body grids. Opt Express. https://doi.org/10.1364/OE.26.015769
27. Carminati C et al (2019) Implementation and assessment of the black body bias correction in quantitative neutron imaging. PLoS ONE. https://doi.org/10.1371/journal.pone.0210300
28. Trtik P, Lehmann EH (2016) Progress in high-resolution neutron imaging at the Paul Scherrer Institut: the neutron microscope project. J Phys Conf Ser. https://doi.org/10.1088/1742-6596/746/1/012004
29. Trtik P, Zubler R, Gong W, Grabherr R, Bertsch J, Duarte LI (2020) Sample container for high-resolution neutron imaging of spent nuclear fuel cladding sections. Rev Sci Instrum 91(5):056103. https://doi.org/10.1063/1.5143226
30. Colldeweih AW et al (2022) Radial delayed hydride cracking in irradiated Zircaloy-2 cladding: advanced characterization techniques. In: ASTM special technical publication 20th international symposium on zirconium in the nuclear industry, accepted